**Accepted Article Preview: Published ahead of online publication**


# Flexible and Robust Te/PET Films for Ultrafast All-Optical Terahertz Modulators

Pujing Zhang, Donggang Xie, Longyu Shi, Haojing Wang, Guangwei She, Wensheng Shi, Peijie Wang, Cunlin Zhang, Kuijuan Jin, Chen Ge and Qingli Zhou

Cite this article as: Pujing Zhang, Donggang Xie, Longyu Shi, Haojing Wang, Guangwei She, Wensheng Shi, Peijie Wang, Cunlin Zhang, Kuijuan Jin, Chen Ge and Qingli Zhou. Flexible and Robust Te/PET Films for Ultrafast All-Optical Terahertz Modulators. *Light: Advanced Manufacturing* accepted article preview 21 May 2026; doi: 10.37188/lam.2026.086



Received 29 December 2025; revised 19 May 2026; accepted 21 May 2026;
Accepted article preview online 21 May 2026

# Flexible and Robust Te/PET Films for Ultrafast All-Optical Terahertz Modulators

**Pujing Zhang[1,2,#], Donggang Xie[3,#], Longyu Shi[1], Haojing Wang[4], Guangwei She[4], Wensheng Shi[4], Peijie Wang[1], Cunlin Zhang[1], Kuijuan Jin[3], Chen Ge[3,*], and Qingli Zhou[1,*]**

[1] Key Laboratory of Terahertz Optoelectronics, Ministry of Education, and Beijing Advanced Innovation Center for Imaging Theory and Technology, Department of Physics, Capital Normal University, Beijing 100048, China

[2] Department of Electrical and Computer Engineering, National University of Singapore, Singapore 117583, Singapore

[3] Beijing National Laboratory for Condensed Matter Physics, Institute of Physics, Chinese Academy of Sciences, Beijing 100190, China

[4] Key Laboratory of Photochemical Conversion and Optoelectronic Materials, Technical Institute of Physics and Chemistry, Chinese Academy of Sciences, Beijing 100190, China

*gechen@iphy.ac.cn

*qlzhou@cnu.edu.cn

## Abstract

Flexible terahertz (THz) devices are fundamental components of wearable photonics and intelligent communication systems. However, conventional THz devices are affected by information loss or signal interruption due to mechanical deformation, which degrade their information fidelity. Here, we introduce tellurium (Te) nanofilms grown on polyethylene terephthalate (PET) substrates as a new class of mechanically robust THz modulators that can successfully improve device performances to optimal levels among existing flexible broadband modulators. The ultrafast transient THz photoresponses of two-dimensional Te films remained unchanged even after 1000 bending cycles or at a small bending radius of 3 mm, exhibiting high tolerance to bending deformation. Furthermore, the variations in the pattern recognition accuracy remained within 2% under different bending conditions, indicating its adaptability to various deformation conditions. This prototype lays the foundation for developing intelligent perception elements that operate stably under complex mechanical deformations.

**Keywords:** terahertz modulator, tellurium nanomaterial, flexible device, mechanical robustness

## Introduction

Terahertz (THz) waves possess potential applications in security imaging, radar stealth, biomedicine, and 6G communications.[1–6] Meanwhile, the development of flexible, broadband, low-cost, and large-area components in optical systems has gained importance with the rapid development of functional THz devices. To meet these requirements, various polymer substrates have been explored for flexible THz devices, such as polyethylene terephthalate (PET), polydimethylsiloxane, and polyimide.[7–10] Among them, PET offers a practical balance among optical transparency, low cost, moisture resistance, dimensional stability, and roll-to-roll compatibility, which are favourable for flexible THz optoelectronic devices.[11,12] The elastic deformability of flexible PET substrates make these THz devices suitable for irregularly shaped surfaces and complex measurement situations that require embedding in curved surfaces, thereby enabling applications in wearable photonic healthcare devices, flexible photodetectors, and chemical and biological sensors.[7–13]

However, flexible all-optical THz modulators face significant challenges in achieving both high performance and mechanical robustness. In practical scenarios, most existing flexible devices undergo structural changes induced by mechanical deformation,[14–21] and fail to meet the stability requirements of communication or imaging applications under arbitrary bending conditions. From the material perspective, current flexible all-optical THz modulators based on two-dimensional (2D) nanofilms face a trade-off between modulation depth and speed.[19–26] Therefore, a novel material with superior photoresponse and mechanical stability is urgently required. As a narrow direct band gap semiconductor, tellurium (Te) nanofilms have attracted extensive interest owing to their excellent optical properties, high carrier mobility, and good ambient stability.[27–29] Notably, Te is consists of atomic chains in a triangular helix, which are stacked together via van der Waals forces in a hexagonal array and possess a one-dimensional (1D) crystal structure.[28,30] Owing to this unique helical chain configuration, Te nanofilms exhibit exceptional mechanical flexibility and high strain tolerance and withstand structural deformation without fracture. Hence, Te nanofilms integrated with flexible substrates are ideal candidates for realising flexible high-performance devices with excellent mechanical robustness.

In this study, we present an all-optical THz modulator based on Te/PET films, which exhibits good flexibility and bending stability. Time-resolved THz spectroscopy

measurements revealed that the Te-based device with broadband and low insertion loss achieved a high modulation depth of 50% on the picosecond timescale and an ultrasensitive response under low pump excitation. In addition, the proposed THz modulator exhibited high tolerance to bending deformation, and the transient photoresponse remained almost unchanged even after 1000 bending cycles or at a bending radius of 3 mm. Furthermore, an artificial neural network (ANN) was constructed for static image processing. The recognition rate based on the Modified National Institute of Standards and Technology (MNIST) handwritten database reached 95%, and the variation range under different bending conditions was only 2%, which was nearly the same order of magnitude as the fluctuation caused by the neural network during the training process. This study provides the foundation for the development of flexible THz-functional devices and offers a promising strategy for establishing next-generation intelligent optoelectronic systems.

## Results and discussion

### Material preparation and characterisation

High-quality and large-area Te nanofilms were deposited by the electron beam evaporation method on PET substrates with thickness of 15 μm. To further confirm the crystal structures of the different domains, high-resolution transmission electron microscopy (HRTEM) was performed (Figure 1a), which directly illustrated the crystalline state of the Te layer with a thickness of approximately 100 nm. In the bottom of Figure 1a, the HRTEM images of a cross-section along the *c*-axis reveal a clear atomic matrix with three-fold symmetry, where each atomic triangle represents a single helical chain. Moreover, the lattice spacing is 0.32 nm from the (101) plane. The Raman spectra are shown in Figure 1b. The prominent peaks located at 93, 122, and 141 $cm^{-1}$ are attributed to the $E_1$, $A_1$, and $E_2$ vibration modes, which originate from asymmetric bond-stretching along *c*-axis and are assigned to bond-bending, chain expansion, and bond-stretching types, respectively.[28] As shown in Figure 1c, the X-ray photoelectron spectroscopy (XPS) spectrum of the Te nanofilm exhibits two obvious peaks with the binding energies of 573.5 and 583.8 eV, which are assigned to Te $3d_{5/2}$ and Te $3d_{3/2}$, respectively.[29–31] Figure 1d illustrates the schematic of the experiment, which uses optical pump-THz probe (OPTP) technology to investigate the active modulation response and mechanical features of Te-based THz devices.

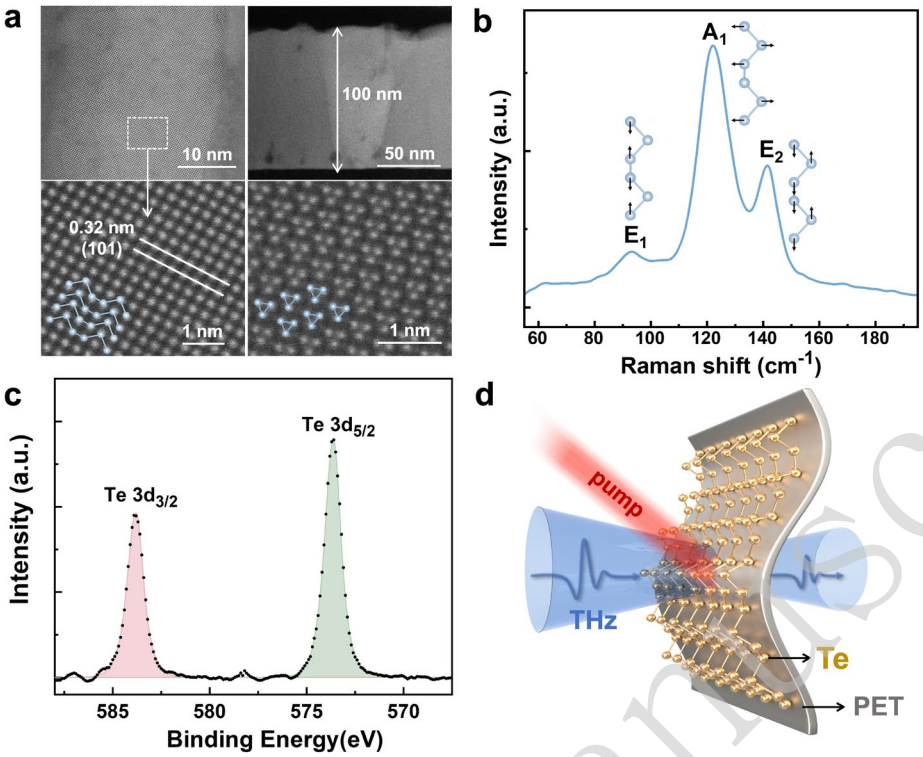


**Figure 1. Material preparation and characterization.** **a** HRTEM images, **b** Raman spectrum, and **c** XPS spectrum of Te nanofilms. **d** Schematic of the THz measurement scheme.

**Transient THz dynamics properties of the device**

The measured transient THz dynamics for Te/PET with 800 nm pump excitation are shown in Figure 2a. The transient THz dynamics of the bare PET substrate exhibit no modulation after photoexcitation, demonstrating that the THz modulation observed in this study originates solely from the Te nanofilm. The relative change is quantified by the modulation depth *MD*, which is defined as a function of the pump delay time *t*: $MD(t) = -\Delta T/T_0 = -(T-T_0)/T_0$, where $T_0$ and $T$ represent the peak THz amplitude before and after the photoexcitation, respectively. The device exhibits a rapid rise in *MD*, reaching its maximum within several picoseconds upon photoexcitation, which is attributed to the generation of hot carriers.[32,33] The subsequent relaxation processes under different pump fluences are satisfactorily fitted by biexponential functions, and the extracted relaxation times $\tau_1$ and $\tau_2$ are displayed in Figure 2b. The fitting function $y = A_1 e^{-\frac{x-x_0}{\tau_1}} + A_2 e^{-\frac{x-x_0}{\tau_2}}$ is used, where $\tau_1$ and $\tau_2$ are the time constants, while $A_1$ and $A_2$ are the corresponding amplitudes, respectively. The fitting parameters were determined based on the physical timescales of the observed decay processes. The decay consists of two stages with distinct timescales. The fast decay $\tau_1$ is due to the energy relaxation

of the carriers, while the slow decay $\tau_2$ depicts the lifetime of the carriers.[34] Fast recovery occurs within 2.5 ps, which represents the energy relaxation of the carriers. This pump-independent trend of $\tau_1$ is attributed to electron-phonon scattering.[35] The slow recovery that lasts for approximately 8.5 ps depicts the carrier lifetime, and its independence of pump fluence suggests that synergistic interactions between the Auger effect and defect trapping dominate the photocarrier dynamics of Te nanofilms.[29,35] The recombination centres formed by impurities and defects promote recombination and shorten the carrier lifetime, whereas the formation of the trap centre prolongs the lifetime. This feature aids in attaining unperturbed modulation speed in optical active devices because the carrier lifetime usually deteriorates with increased pump intensity. The $MD(t=0)$ of Te is 5.5%, even at an extremely low power of 1 mW, and reaches 50.8% at 100 mW, while the corresponding transmission spectra at a pump delay time of 0 ps exhibit fluence-dependent, but frequency-independent broadband features (Supplementary Figure S1). The high transmission of this material (approximately 96.1% without the pump) leads to a very low insertion loss of −0.35 dB calculated by $20\lg(E_{sam}/E_{sub})$, where $E_{sam}$ and $E_{sub}$ are the THz amplitudes for the sample and substrate, respectively. Figure 2c presents a comprehensive performance comparison between the Te/PET device and other flexible THz modulators based on 2D nanomaterials (see Table S1 for details).[14–26] For instance, $VO_2$-based devices exhibit high *MD* within milliseconds. Conversely, modulators with graphene (Gr) or Ge, which exhibit ultrafast picosecond responses, possess limited modulation efficiencies. The Te/PET device presented in this work successfully attained optimal indices with a high *MD* of 50.8% and an ultrafast picosecond response in current flexible nanofilm components, suggesting a potential modulation speed of tens of GHz range. These parameters are relevant to communication and imaging applications. Specifically, high modulation ensures reliable amplitude encoding; picosecond response time corresponds to potential high-speed modulation capability; while low insertion loss and broadband response guarantee efficient signal transmission with minimal distortion.

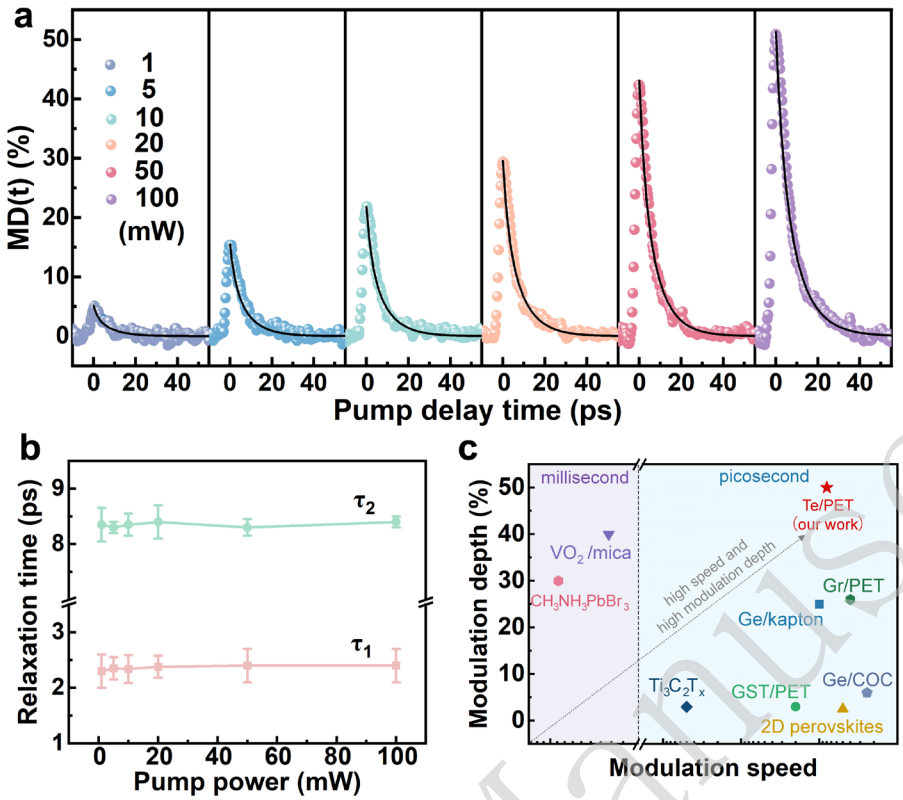


**Figure 2. Transient dynamics properties of Te/PET. a** Transient THz dynamics of Te/PET under different pump powers at an excitation wavelength of 800 nm. The black solid lines represent the biexponential fitting curves. **b** Pump power dependence of the fitted relaxation times. **c** Performance comparison of optical flexible THz modulators among the 2D nanofilms.

**Bending tolerance of the proposed device**

As shown in Figure 3a, we first examined the photoresponse stability of the device in the flat state after 1000 illumination cycles (on/off = 1/1s) at a pump power of 20 mW and delay time of 0 ps. *MD* remains constant without degradation, indicating excellent durability and reproducibility. These results reflect the operational stability of the device performance under repeated optical excitation and can serve as a baseline test for communication or imaging systems. In this mapping, the optically controlled off and on states correspond to digital 0 and 1 in THz communication or low- and high-intensity pixels in imaging applications. The unchanged THz modulation depth after 1000 on/off cycles indicates excellent robustness and demonstrates that the device operates stably under both high-frequency and long-term working conditions. In addition, the Te/PET films exhibited excellent spatial uniformity and long-term ambient stability, ensuring the robustness of the device (Supplementary Figures S2 and S3). We

further studied the transient THz dynamic properties of the flexible Te nanofilms under various bending conditions at the same pump power. During these measurements, the flexible Te/PET device was fixed on a copper bar and bent to any state. Figure 3b presents the experimental results under bending deformation with radii of 8, 5, and 3 mm. We then examined the bending cyclability for 100, 500, and 1000 times with a bending radius of 6 mm, as shown in Figure 3c. The transient THz dynamics curves of the Te nanofilm do not exhibit obvious variations under different bending radii and cycles compared to those in a flat state. The modulation performance remained stable even after 10000 bending cycles (Supplementary Figure S4). This excellent mechanical robustness can be attributed to the unique quasi-1D crystal structure of Te.[27,28] Unlike isotropic bulk crystals, the trigonal Te lattice comprises stacked helical atomic chains spiralling along the *c*-axis, which are stacked together via weak van der Waals interactions. Under bending deformation, these weak interchain forces allow stress relaxation through slight chain reorientation or sliding to prevent structural fracture.[27] In addition, the Raman spectra were utilised to investigate the effect of bending states on the lattice structure (Supplementary Figure S5). The three characteristic vibrational peaks exhibited no obvious shifts, indicating that the Te nanofilm maintained its high structural integrity and original crystalline state without significant lattice distortion during the bending process. The robustness of the Te/PET device was further proved by the small tensile strain of 0.25%, which was considerably less than the strain limit because the tensile strain is the ratio of the whole sample thickness (15.1 μm) to the bending radius (3 mm).[36–39] The bending durability is particularly important for flexible devices and is a primary index of device degradation. Therefore, we performed mechanical measurements on the device under different bending radii (8, 5, and 3 mm), as shown in Figs. 3d–f. After 1000 cycles, the transient photoresponse properties at $t$=0 fluctuate negligibly for all bending radii. Furthermore, these key metrics remain nearly unchanged under different bending radii and after repeated bending cycles, indicating that the device maintains stable modulation output even under mechanical deformation and complex physical environments. This robustness against mechanical fatigue further confirms that Te/PET devices are ideal for practical applications.

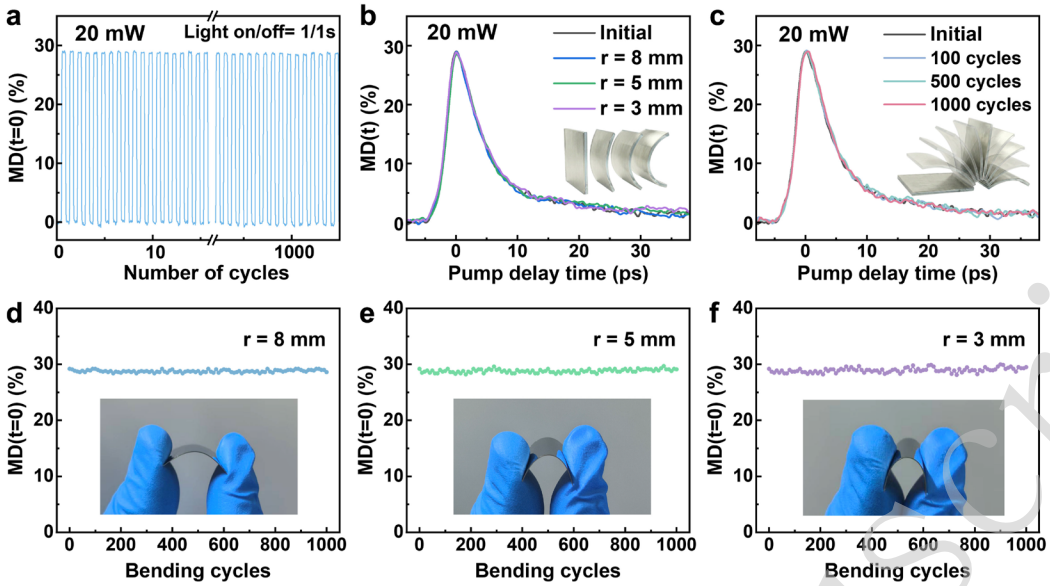


**Figure 3. Mechanical flexibility and durability of device. a** Optical switching stability measurement under initial state over 1000 illumination cycles at pump delay time $t$=0. **b** Transient THz dynamics curves of Te nanofilm under different bending radii (8, 5, and 3 mm) and **c** for different bending cycles (100, 500, 1000) at a bending radius of 6 mm. **d-f** Transient photoresponse properties ($t$=0) for 1000 bending cycles under different bending radii. The insets display photographs of the bending equipment.

### Mechanical robustness and demonstration of neuromorphic computing

Unlike conventional devices that often suffer from signal interruption or destruction under mechanical deformation, the proposed device maintains robust information transmission capabilities, as illustrated in Figure 4a. Figure 4b shows the potentiation and depression behaviours with incremental light pulses of 3–100 mW under the flat and bending states. The *MD*s of the devices change regularly with the number of applied pulses. The device states can be reversibly programmed between high and low conductance levels by actively controlling the optical input. The results demonstrate that the device presents a continuously adjustable *MD* regardless of bending deformation. The photoresponse behaviours in the six bending states are consistent with those in the flat state, confirming the good bending tolerance of the device. In addition, ensuring stable information fidelity under mechanical deformation conditions is essential. The extracted response profiles of the initial and bent states at 5 mm indicated that all the devices maintained an ultrafast response time of approximately 8 ps and preserved symmetric and linear photoresponse features without distortion (Figure 4c). These characteristics are crucial for the recognition accuracy of simulations. To explore the feasibility of the proposed devices for neuromorphic computing, a typical ANN was

established to test the MNIST database. The grey value (0–255) of each pixel in a handwritten digit image was linearly mapped to the THz pump power (0–100 mW), and 784 sensory neurons were used to sense the stimuli and encode them into different *MD*s. The mapping relationship between the THz pump power and encoded *MD* is shown in Figure S6. The input information, *MD*, was then read as the modulated THz amplitude by the probe pulse and fed into a three-layer ANN consisting of 784 input, 300 hidden, and 10 output neurons for processing. The stimuli images were classified into 10 different categories after training the network. Figures 4d and 4e show the evolution of the test accuracy during the training process for the three bending radii and cycles, respectively. The recognition accuracy remains stable at approximately 95% with a variation range of only 2% under the bending conditions after 30 training epochs, which is similar to the fluctuation caused by the neural network itself during training. Figure 4f shows the confusion matrix of the classification results for 10,000 test images after 30 epochs at a bending radius of 3 mm. The columns designate the actual labels of the stimuli images; the rows represent the inferred results; and the colour bars indicate the number of instances. The confusion matrix for the other bending conditions is shown in Figure S7. The results verified that the mechanical robustness of the device was effectively translated into high-performance pattern recognition. The conceptual demonstration of pattern classification suggests the proposed flexible device can be used for object recognition, indicating its great potential for use in intelligent optoelectronic devices.

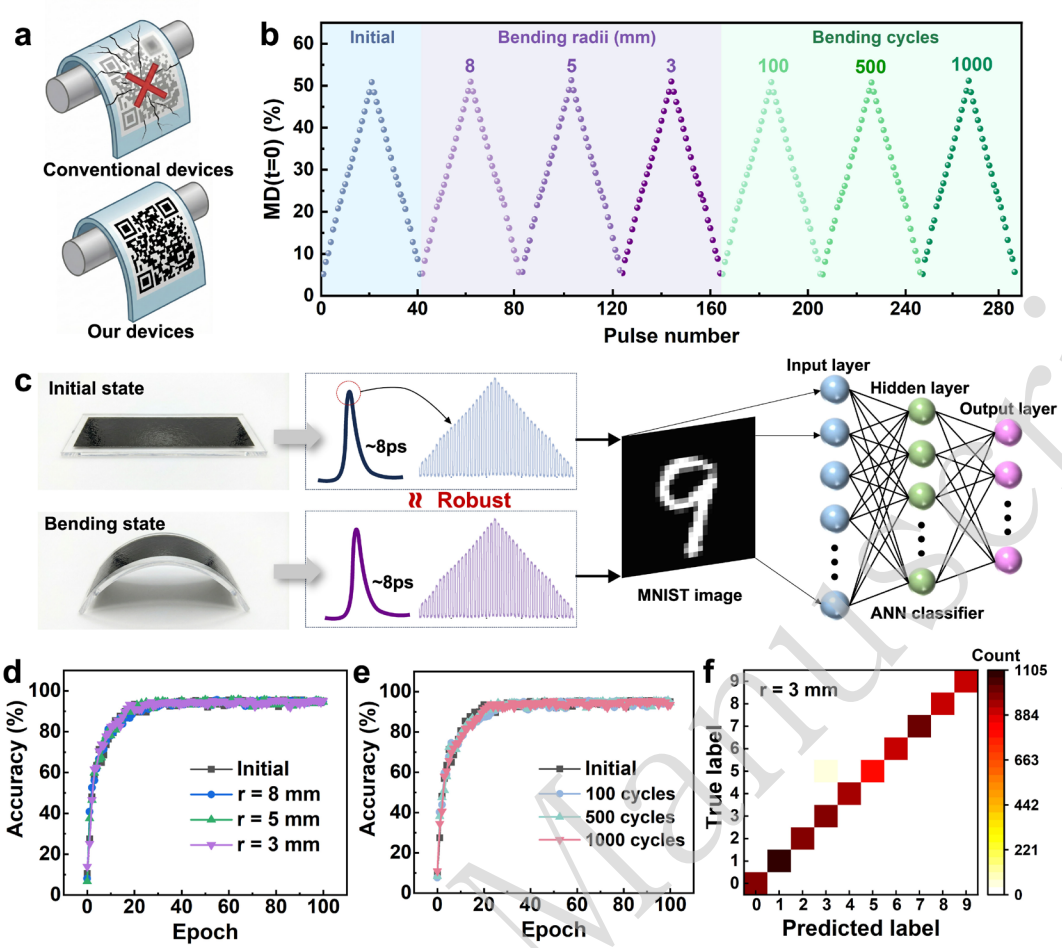


**Figure 4. Application of the flexible Te/PET modulator in neuromorphic computing. a** Schematic comparison of the mechanical durability of conventional devices and the proposed Te/PET device. **b** Measured *MD* with incremental light pulse under different conditions. **c** Schematic of the ANN-based image recognition simulation. **d** Recognition accuracy of the ANN classifier under different bending radii and **e** after different bending cycles. **f** Confusion matrix of the classification results of the test dataset after 30 epochs at a bending radius of 3 mm.

## Conclusion

In summary, we used Te nanofilms on a PET substrate to demonstrate a high-performance flexible and mechanically robust THz modulator. This device achieved optimal indices with a high modulation efficiency (50% *MD*) and picosecond-level ultrafast speed (8 ps) in existing flexible 2D material systems. Notably, the modulation performance remained unchanged under bending deformation even at a bending radius of 3 mm and 1000 bending cycles. Furthermore, we constructed an ANN consisting of the proposed devices for static image processing and successfully achieved a recognition function in the THz band. The recognition accuracy of the MNIST handwritten database reached 95%, and the variation range under different bending

conditions was only 2%, further demonstrating that the proposed device possessed excellent mechanical stability. Such mechanically robust Te-based THz devices offer a promising solution for efficient pattern-recognition systems and lay the foundation for the development of flexible intelligent optoelectronic devices with neuromorphic functions.

## Materials and methods

### Sample preparation

The Te nanofilms were grown on PET substrates in an electron-beam evaporator (VZS 600 Pro) with an *in situ* thickness meter. Before deposition, the PET substrates were cleaned via ultrasonication in acetone for 10 min and rinsed with isopropyl alcohol and deionised water. Te deposition was initiated from a 99.999% pure Te source in a boron nitride crucible at a rate of 0.1 nm $s^{-1}$ under $10^{-4}$ Pa pressure. Annealing was performed in a tube furnace at 373 K under 100 sccm Ar atmosphere for 0.5 h.

### Material characterisation

HRTEM was performed using a Cs-corrected JEOL JEMARM200CF NEOARM instrument operated at 200 kV with a CEOS Cs corrector (CEOS GmbH, Heidelberg, Germany). Raman spectra were analysed using an alpha300 R microscope under 532 nm laser excitation. XPS measurements were performed on ThermoFisher Scientific ESCALAB 250X under monochromatic Al Kα radiation with energy of 1486.6 eV.

### Optical pump-THz probe measurements

The 800 nm source beam with a 100 fs duration and 1 kHz repetition rate delivered by a Spectra Physics regenerative amplifier was divided into three paths to generate THz waves, probe the THz signal, and pump the samples. First, the transmitted THz signals were measured by blocking the pump beam. A 1D pump curve was then obtained by scanning the pump delay line with the THz generation delay line at a fixed position at the peak of the THz pulse. The spot size of the pump beam was approximately 0.3 $cm^2$. In our OPTP measurements, the zero point of the pump delay time was defined as the maximum *MD*, corresponding to the greatest pump-induced change in the peak THz amplitude. This point represents the time at which the optical pump and THz probe pulses encounter each other in the sample.

### Simulation of pattern recognition

The ANN combined with a Te-based THz device consisted of an input layer, a hidden

layer, and an output layer with 784, 300, and 10 nodes, respectively. The backpropagation algorithm was used for the training process, and the weight update rule was defined using the experimental potentiation and depression data shown in Figure 4b. The activation functions of the hidden and output layers are Sigmoid and Softmax, respectively.

**Acknowledgements**

We thank Prof. Cheng-Wei Qiu for the discussions and comments. This study was supported by the National Key R&D Program of China (No. 2024YFA1409500), Postdoctoral Fellowship Program of CPSF (GZC20252257), Beijing Natural Science Foundation (Nos. 4264139 and 4262076), China Postdoctoral Science Foundation (2025M783418), Beijing Postdoctoral Science Foundation (pc-2025-06), National Natural Science Foundation of China (Nos. 62075142 and 12222414), and Youth Innovation Promotion Association of CAS (No. Y2022003).

**Author contributions**

P.Z. and Q.Z. conceived the idea and directed the project. C.G. supervised the study. P.Z. and L.S. performed sample preparation, device fabrication, and measurements. D. X. performed the simulations. H.W. and G.S. conducted the characterisation. All the authors discussed the results and commented on the paper.

**Data availability**

All relevant data are available within the Article and Supplementary Information or from the corresponding authors upon reasonable request.

**Competing interests**

The authors declare no competing interests.

**Supplementary information**

Supplementary materials are available at the online version.

## References

1. Katyba, G. M. et al. Terahertz endoscopy of hard-to-access objects in the context of neoplasms diagnosis-A review. *Light*: *Advanced Manufacturing* **6**, 58 (2025).
2. Stantchev, R. I. et al. Noninvasive, near-field terahertz imaging of hidden objects using a single-pixel detector. *Science Advances* **2**, e1600190

(2016).
3. Wang, H. Y. et al. Compatibility challenges and strategies of multispectral stealth materials: from microwave-terahertz absorption to infrared camouflage. *Advanced Materials Technologies* **11**, e01616 (2026).
4. Wang, Y. et al. Recent advances in metasurfaces: from THz biosensing to microwave wireless communications. *Research* **8**, 0820 (2025).
5. Wang, S. J. et al. Flexible generation of structured terahertz fields via programmable exchange-biased spintronic emitters. *eLight* **4**, 11 (2024).
6. Alsharif, M. H. et al. Toward 6G communication networks: terahertz frequency challenges and open research issues. *Computers*, *Materials & Continua* **66**, 2831-2842 (2021).
7. Zhang, T. Y. et al. All-in-one flexible MXene/PET films via scalable scanning centrifugal casting for high transparency and ultra-wide multispectral electromagnetic responses. *Advanced Science* **12**, 2501540 (2025).
8. Yang, W. G. et al. Recent advances in the development of flexible sensors: mechanisms, materials, performance optimization, and applications. *Journal of Electronic Materials* **51**, 6735-6769 (2022).
9. Li, X. T. et al. Metasurface-driven sensing in terahertz region: principles, applications, fabrication, and challenges. *Advanced Materials Technologies* **10**, e00886 (2025).
10. Zhang, M. W. et al. Bionic artificial skin based on self-healable ionogel composites with tailored mechanics and robust interfaces. *Advanced Materials* **36**, 2405776 (2024).
11. Hassan, M. et al. Significance of flexible substrates for wearable and implantable devices: recent advances and perspectives. *Advanced Materials Technologies* **7**, 2100773 (2022).
12. Korotcenkov, G. The Handbook of Paper-Based Sensors and Devices. (Cham: Springer, 2025).
13. Park, H. et al. Organic flexible electronics with closed-loop recycling for sustainable wearable technology. *Nature Electronics* **7**, 39-50 (2024).
14. Peng, S. et al. Thermal and mechanical THz modulation of flexible all-dielectric metamaterial. *Optics Express* **31**, 2644-2653 (2023).
15. Shi, Q. W. et al. Flexible and giant terahertz modulation based on ultra-strain-sensitive conductive polymer composites. *ACS Applied Materials & Interfaces* **12**, 9790-9796 (2020).
16. Zhang, C. H. et al. A printed flexible broad-band THz absorber based on 2D $Ti_3C_2T_x$ MXene. *Applied Surface Science* **710**, 163956 (2025).
17. Ouyang, W. C. et al. Ultrathin-flexible multifunctional MXene composite hydrogels with good mechanical properties-high strain sensitivity and ultra-broadband EMI shielding performances. *Chemical Engineering Journal* **494**, 153068 (2024).
18. Feng, T. D. et al. Highly flexible $Ti_3C_2T_x$ MXene/waterborne polyurethane membranes for high-efficiency terahertz modulation with low insertion loss.

*ACS Applied Materials & Interfaces* **15**, 7592-7601 (2023).
19. Cheng, L. et al. Mechanical terahertz modulation based on single-layered graphene. *Advanced Optical Materials* **6**, 1700877 (2018).
20. Chang, X. et al. Impact of the uniaxial strain on terahertz modulation characteristics in flexible epitaxial $VO_2$ film across the phase transition. *Optics Express* **31**, 13243-13254 (2023).
21. Pitchappa, P. et al. Volatile ultrafast switching at multilevel nonvolatile states of phase change material for active flexible terahertz metadevices. *Advanced Functional Materials* **31**, 2100200 (2021).
22. Li, G. J. et al. Dynamical control over terahertz electromagnetic interference shielding with 2D $Ti_3C_2T_y$ MXene by ultrafast optical pulses. *Nano Letters* **20**, 636-643 (2020).
23. Lim, W. X. et al. Ultrafast all-optical switching of germanium-based flexible metaphotonic devices. *Advanced Materials* **30**, 1705331 (2018).
24. Fan, X. C. et al. Highly deformable and high-performance optical paper-based perovskite terahertz modulator. *Optics Express* **33**, 7978-7988 (2025).
25. Kumar, A. et al. Excitons in 2D perovskites for ultrafast terahertz photonic devices. *Science Advances* **6**, eaax8821 (2020).
26. Wang, K. M. et al. Nanometric Ge films for ultrafast modulation of THz waves with flexible metasurface. *Advanced Optical Materials* **12**, 2402010 (2024).
27. Shi, Z. et al. Two-dimensional tellurium: progress, challenges, and prospects. *Nano-Micro Letters* **12**, 99 (2020).
28. Wang, Y. X. et al. Field-effect transistors made from solution-grown two-dimensional tellurene. *Nature Electronics* **1**, 228-236 (2018).
29. Zhang, P. J. et al. High-performance terahertz modulators induced by substrate field in Te-based all-2D heterojunctions. *Light*: *Science & Applications* **13**, 67 (2024).
30. Peng, J. et al. Two-dimensional tellurium nanosheets exhibiting an anomalous switchable photoresponse with thickness dependence. *Angewandte Chemie International Edition* **57**, 13533-13537 (2018).
31. Zheng, B. N. et al. Large-area tellurium/germanium heterojunction grown by molecular beam epitaxy for high-performance self-powered photodetector. *Advanced Optical Materials* **9**, 2101052 (2021).
32. Dai, Z. J. et al. High mobility 3D Dirac semimetal ($Cd_3As_2$) for ultrafast photoactive terahertz photonics. *Advanced Functional Materials* **31**, 2011011 (2021).
33. Xu, S. J. et al. Transient photoconductivity and free carrier dynamics in a monolayer $WS_2$ probed by time resolved Terahertz spectroscopy. *Nanotechnology* **30**, 265706 (2019).
34. Srivastava, Y. K. et al. $MoS_2$ for ultrafast all-optical switching and modulation of THz Fano metaphotonic devices. *Advanced Optical Materials* **5**, 1700762 (2017).

35. Xing, X. et al. Role of photoinduced exciton in the transient terahertz conductivity of few-layer $WS_2$ laminate. *The Journal of Physical Chemistry C* **121**, 20451-20457 (2017).
36. Li, D. et al. Ultrafast dynamics of defect-assisted auger process in $PdSe_2$ films: synergistic interaction between defect trapping and auger effect. *The Journal of Physical Chemistry Letters* **13**, 2757-2764 (2022).
37. Han, S. T., Zhou, Y. & Roy, V. A. L. Towards the development of flexible non-volatile memories. *Advanced Materials* **25**, 5425-5449 (2013).
38. Ren, Y. et al. Gate-tunable synaptic plasticity through controlled polarity of charge trapping in fullerene composites. *Advanced Functional Materials* **28**, 1805599 (2018).
39. Li, G. et al. Flexible $VO_2$ films for in-sensor computing with ultraviolet light. *Advanced Functional Materials* **32**, 2203074 (2022).